Biosensors

DOI: 10.1002/ange.201302481

Sub-10 nm Lanthanide-Doped CaF_2 Nanoprobes for Time-Resolved Luminescent Biodetection**

*Wei Zheng, Shanyong Zhou, Zhuo Chen, Ping Hu, Yongsheng Liu, Datao Tu, Haomiao Zhu, Renfu Li, Mingdong Huang, and Xueyuan Chen**

Lanthanide-doped luminescent nanoparticles (NPs) have evoked considerable interest due to their superior features, such as sharp f–f emission peaks, a long photoluminescence (PL) lifetime, low toxicity, and high resistance to photobleaching, which make them extremely suitable for use as alternatives to organic fluorescent dyes or quantum dots for various bioapplications.[1] Particularly for in vivo bioimaging, there are some rigorous requirements for bioprobes, such as bright luminescence, small size, and biosafety.[2] The use of sub-10 nm NPs enables free access to intracellular compartments and better clearance.[2c] For in vitro biodetection, sub-10 nm nanoprobes are highly desired for homogeneous bioassays based on distance-dependent fluorescence resonance energy transfer (FRET).[3]

Fluorides, owing to their high chemical stability and intrinsic low phonon energies ($< 350\ cm^{-1}$), are considered as the most efficient host materials for lanthanide (Ln^{3+}) doping to achieve desirable upconversion (UC) or downshifting (DS) luminescence.[4] Among Ln^{3+}-doped fluoride NPs, calcium fluoride exhibits excellent biocompatibility.[5] Currently, owing to the surface quenching effect, it remains a challenge to synthesize ultrasmall CaF_2:Ln^{3+} NPs that are highly emissive.[6] Meanwhile, it is also difficult to control the morphology of CaF_2 NPs when heterovalently doped with Ln^{3+} emitters in various amounts.[7] Therefore, the development of an effective strategy for the fabrication of monodisperse and small-sized CaF_2:Ln^{3+} NPs with intense PL and diverse Ln^{3+} doping compositions for various bioapplications, such as time-resolved (TR) PL biodetection and targeted bioimaging, is urgent. The TRPL assay, which eliminates the interference of scattered light and other short-lived autofluorescence from cells and tissues through time-resolved detection, provides a background-free signal and thus offers remarkably high sensitivity relative to that of conventional fluorescence immunoassays.[8] Most previous TRPL or TR-FRET bioassays have been restricted to the use of molecular probes, such as Ln^{3+} chelates.[8a] Only a few TR nanoprobes based on Ln^{3+}-doped inorganic NPs have been explored until recently; however, such probes are limited to the detection of avidin.[9] The use of Ln^{3+}-doped inorganic nanoprobes for the TRPL detection of tumor markers, such as urokinase plasminogen activator receptor (uPAR), which is an important type of tumor marker and over-expressed in a variety of human cancer cells,[10] remains untouched so far.

Herein, we develop a strategy based on sodium codoping for the synthesis of monodisperse and ultrasmall CaF_2:Ln^{3+} (Ln = Ce, Tb; Yb, Er; Yb, Tm) NPs through a coprecipitation route. We reveal the role of the sodium ion as a nucleator and charge compensator in the synthesis and its importance for the growth and optical properties of the NPs. The resulting sub-10 nm CaF_2:Ln^{3+} core-only and core/shell NPs with tunable shell thickness yielded enhanced DS and UC luminescence (UCL). By utilizing ultrasmall CaF_2:Ce,Tb nanoprobes and their intense long-lived PL, we demonstrate the sensitive detection of avidin in homogeneous TR-FRET and heterogeneous TRPL bioassays. Finally, we describe the use of these nanoprobes as sensitive TR-FRET probes for the detection of the tumor marker uPAR and in uPAR-targeted cancer-cell imaging.

High-quality CaF_2:Ln^{3+} core-only and core/shell NPs were synthesized through a coprecipitation route. The as-synthesized NPs were hydrophobic and could be dispersed readily in a variety of nonpolar organic solvents, such as cyclohexane. The resulting transparent colloidal solution (Figure 1a) displayed intense green emission under irradiation at 280 nm with an ultraviolet (UV) laser (Ce,Tb-doped NPs), or yellow (Yb,Er-doped NPs) or blue emission (Yb,Tm-doped NPs) under irradiation at 980 nm with a near-infrared (NIR) laser (Figure 1b–d). TEM analysis showed that the as-synthesized CaF_2:Yb,Er core-only NPs were roughly spherical with an average diameter of (3.8 ± 0.5) nm, as corroborated by the markedly broadened X-ray diffraction (XRD) peaks (Figure 1e; see also Figure S1 in the Supporting Information). The corresponding high-resolution TEM (HRTEM) image clearly shows the high crystallinity of the NPs (Figure 1i). The lattice fringes are very clear with an observed d spacing of 0.31 nm, which is in good agreement with the lattice spacing of the (111) plane of cubic-phase CaF_2

[*] Dr. W. Zheng, Dr. Y. S. Liu, Dr. D. T. Tu, Dr. H. M. Zhu, R. F. Li, Prof. X. Y. Chen
Key Laboratory of Optoelectronic Materials Chemistry and Physics
Fujian Institute of Research on the Structure of Matter
Chinese Academy of Sciences, Fuzhou, Fujian 350002 (China)
E-mail: xchen@fjirsm.ac.cn
S. Y. Zhou, Dr. Z. Chen, P. Hu, Prof. M. D. Huang
State Key Laboratory of Structural Chemistry and
Danish–Chinese Centre for Proteases and Cancer
Fujian Institute of Research on the Structure of Matter
Chinese Academy of Sciences, Fuzhou, Fujian 350002 (China)

[**] We thank Prof. Fuyou Li and Qian Liu for the cellular-imaging experiment. This research was supported by the NSFC (Nos. 11004191, 51102234, 11204302, and 31161130356), the 863 Program of MOST (No. 2011AA03A407), the Special Project of National Major Scientific Equipment Development of China (No. 2012YQ120060), the Scientific Equipment Development Project of CAS (No. YZ201210), and the NSF of Fujian Province for Young Scientists (Nos. 2012J05106 and 2011J05145).

Supporting information for this article is available on the WWW under http://dx.doi.org/10.1002/anie.201302481.

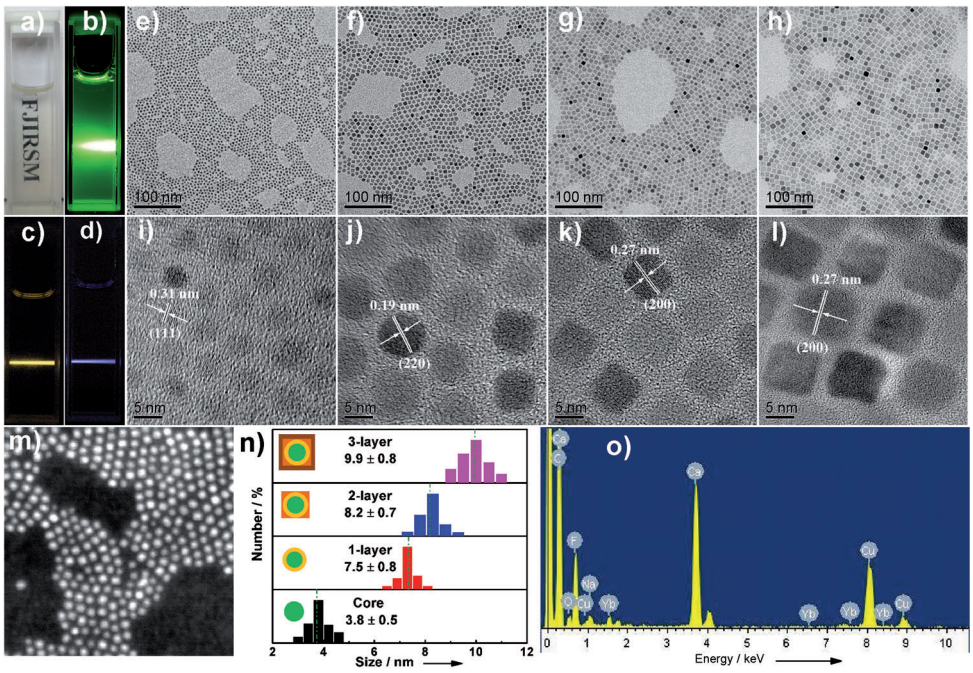

Figure 1. a) Photograph showing the transparency of the as-prepared CaF_2:Ln^{3+} (Ln = Ce, Tb; Yb, Er; Yb, Tm) NPs dispersed in cyclohexane. b) DS-luminescence photograph of the as-prepared CaF_2:Ce,Tb NPs dispersed in cyclohexane under laser irradiation at 280 nm. c,d) UCL photographs of the as-prepared 1-ML CaF_2:Yb,Er@CaF_2 (c) and CaF_2:Yb,Tm@CaF_2 core/shell NPs (d) dispersed in cyclohexane under NIR laser irradiation at 980 nm. e–h) TEM and i–l) HRTEM images of the as-prepared CaF_2:Yb,Er core-only (e,i) and 1-ML (f,j), 2-ML (g,k), and 3-ML core/shell NPs (h,l). m) HAADF-STEM image of 1-ML CaF_2:Yb,Er@CaF_2 core/shell NPs. n) Size distribution of CaF_2:Yb,Er core-only and core/shell NPs as obtained from 200 particles in the TEM images. o) EDS pattern of CaF_2:Yb,Er core-only NPs.

(JCPDS no. 87-0971). Compositional analysis by energy-dispersive X-ray spectroscopy (EDS) and inductively coupled plasma atomic emission spectroscopy revealed the existence of Ca, F, and the doping Na, Yb, and Er ions in CaF_2:Yb,Er core-only NPs (Figure 1 o; see also Table S1 in the Supporting Information). Interestingly, no noticeable variations in the size and morphology of the NPs were observed when the Ln^{3+} content or the solvent ratio used in the synthesis was changed (see Figures S1–S4), in remarkable contrast to the solvothermal method,[7] for which Ln^{3+} doping was found to significantly change the size and morphology of the NPs. However, we found that the codopant Na^+ may play an important role in the crystallization of the NPs: Codoping with Na^+ promoted the nucleation process and enhanced the crystallinity of the resulting NPs (see Figures S5 and S6).

Besides core-only NPs, core/shell NPs with superior UCL could be obtained through epitaxial layer-by-layer (LBL) growth. TEM images showed an increase in the particle size of CaF_2:Yb,Er@CaF_2 core/shell NPs obtained by coating with 1-, 2-, and 3-monolayer (ML) CaF_2 shells (Figure 1 f–l). During LBL shell growth, the size of the core/shell NPs grew gradually from (3.8 ± 0.5) nm (core-only) to (7.5 ± 0.8) nm (1-ML), (8.2 ± 0.7) nm (2-ML), and (9.9 ± 0.8) nm (3-ML); the increasing size of the nanoparticles is in line with their narrower XRD peaks (Figure 1 n; see also Figure S7). The corresponding HRTEM images exhibit clear lattice fringes with observed *d* spacings of 0.19 nm for the (220) plane and 0.27 nm for the (200) plane and thus indicate the high crystallinity of core/shell NPs (Figure 1 j–l). A high-angle annular dark-field scanning TEM (HAADF-STEM) image of the 1-ML CaF_2:Yb,Er@CaF_2 core/shell NPs shows a discernible contrasted core/shell structure (Figure 1 m). In this image, the brighter regions correspond to the heavier Yb^{3+} ions in the cores, and the darker regions correspond to the lighter Ca^{2+} ions in the shells.

Figure 2 shows the emission spectra, excitation spectra, and PL decay for CaF_2:Ce,Tb NPs synthesized with different Na^+ concentrations. Upon excitation at 304 nm, a characteristic Tb^{3+} emission assigned to the $^5D_4 \rightarrow {}^7F_{1-6}$ transition was detected (Figure 2 a). The overall PL intensity was enhanced remarkably as the Na^+ concentration increased. Typically, the PL intensity of NPs synthesized with Na^+ at a concentration of 2.5 mM was approximately 34 times that of the sodium-free NPs. The absolute quantum yield, defined as the ratio of the number of emitted photons to the number of absorbed photons, increased from (9 ± 1) to (51 ± 1) %. This improvement could be attributed to: 1) the aforementioned enhanced

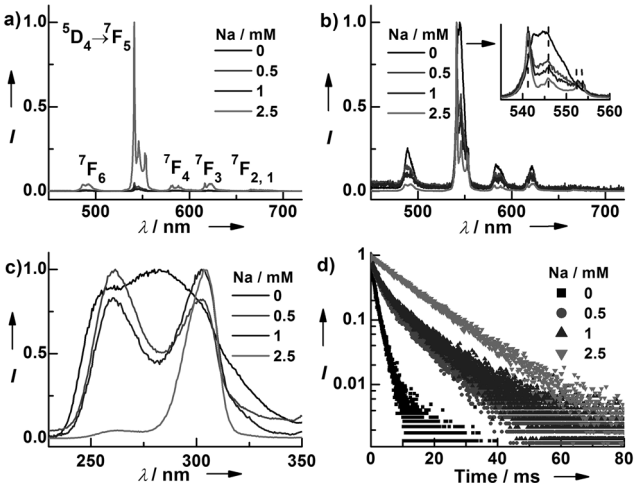

Figure 2. a) PL emission spectra and b) the corresponding normalized emission spectra of CaF_2:5 % Ce^{3+},5 % Tb^{3+} NPs synthesized with different Na^+ concentrations upon excitation at 304 nm. c) Normalized PL excitation spectra and d) PL decay from $^5D_4$ by monitoring the Tb^{3+} emission at 541.2 nm for NPs synthesized with different Na^+ concentrations.

crystallinity of the NPs; 2) reduced concentration quenching of Tb^{3+} as a result of charge compensation by Na^+;[11] and 3) modification of the crystal-field environment of the emitters, as evidenced by the marked changes in the excitation bands for the transitions from the ground state to the 5d state of Ce^{3+} as the Na^+ concentration was increased (Figure 2c). Furthermore, unusual sharp spectral-line splitting and an enhanced $^5D_4 \rightarrow {}^7F_5/{}^5D_4 \rightarrow {}^7F_{6,4,3,2,1}$ fluorescence branching ratio were observed for Na^+-codoped NPs (Figure 2b). The $^5D_4$ decay of Tb^{3+} varied from non-single-exponential decay in the sodium-free NPs to single-exponential decay in NPs synthesized with Na^+ (2.5 mM), and the corresponding effective PL lifetime was prolonged from about 1.25 to about 12.0 ms (Figure 2d). These results further confirmed the drastically different crystal-field environment around the Ln^{3+} dopants. To the best of our knowledge, such a long PL lifetime, which is favorable for FRET-based biodetection in vitro and bioimaging in vivo, has not been reported in such small NPs before. Besides improved DS luminescence, enhanced UCL was also observed for the CaF_2:Yb,Er@CaF_2 (and CaF_2:Yb,Tm@CaF_2) core/shell NPs: the UCL intensity and lifetime of Er^{3+} (or Tm^{3+}) were found to increase markedly as the number of MLs increased (see Figures S8 and S9).

To render the hydrophobic CaF_2:Ln^{3+} NPs biocompatible, we modified their surface with a hydrophilic ligand through a ligand-exchange procedure.[12] 2-Aminoethyl dihydrogen phosphate (AEP) was used to replace the native hydrophobic ligands on the surface of the NPs. The successful attachment of AEP to the surface of the NPs was established by Fourier transform infrared (FTIR) spectroscopy and thermogravimetric analysis (see Figures S10 and S11). These AEP-capped NPs showed much better water solubility (see Figure S12). More importantly, AEP-capped CaF_2:Ce,Tb NPs preserved the intense long-lived luminescence of their parent NPs with a nearly unaltered PL lifetime of approximately 12.5 ms (see Figure S13), which is the longest known for Tb^{3+}-based TR luminescent bioprobes (see Table S2). In contrast to the short-lived autofluorescence of biological tissues or organic dyes, the long-lived PL of Ln^{3+} can be distinguished readily from the undesired background fluorescence by means of TR detection (see Figure S14). For further biological applications, AEP-capped NPs were conjugated to capture molecules, such as biotin or the amino terminal fragment (ATF) of urokinase plasminogen activator (uPA), which can bind specifically to the analytes avidin ($K_d \approx 10^{-6}$ nM) and uPAR (uPA receptor, $K_d \approx 0.28$ nM), respectively.[13] We conjugated biotin and ATF to the surface of NPs by a recently developed facile method.[9a] The formation of amide bonds, as evidenced by FTIR spectroscopy, and the different ζ potentials for aqueous solutions (pH 6.9) of AEP-capped, biotinylated, and ATF-coupled NPs revealed the successful conjugation of biotin or ATF to the surface of the NPs (see Figures S10 and S15).

After conjugation with biotin, CaF_2:Ce,Tb NPs were further explored as heterogeneous TRPL bioprobes in an avidin–biotin model. The process for a TRPL assay is depicted in Figure 3a. Avidin was quantified by measurement of the PL intensity of the NPs that were conjugated to avidin (which was itself bound to the wells) through specific binding

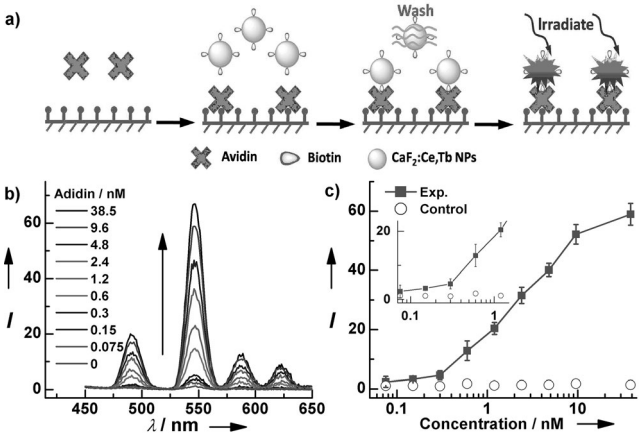

Figure 3. a) Schematic representation of the heterogeneous TRPL detection of avidin. b) TRPL spectra of the bioassays with biotinylated CaF_2:Ce,Tb NPs as probes as a function of the avidin concentration. c) Calibration curve for TRPL detection: integrated PL intensity versus the concentration of avidin. The control experiment was conducted with nonbiotinylated NPs as the bioprobes.

between avidin and biotin. The observed TRPL signal was gradually enhanced as the amount of avidin was increased (Figure 3b). For comparison, we conducted nonbinding control experiments by replacing the biotinylated NPs (or avidin) with AEP-capped NPs (or bovine serum albumin (BSA)) under otherwise identical conditions; in this case, the TRPL signal was hardly detectable (see Figure S16). The calibration curve for the TRPL detection of avidin exhibits a nearly linear dependence in the range of 0.3–10 nM and tends to saturate when the concentration exceeds 10 nM. The limit of detection (LOD), defined as the concentration that corresponds to 3 times the standard deviation above the signal measured in the control experiment, reached a record low value of approximately 48 pM.[8b]

A homogeneous TR-FRET assay with ultrasmall CaF_2:Ce,Tb NPs was also explored. Fluorescein isothiocyanate (FITC) and CaF_2:Ce,Tb NPs were selected as acceptor and donor labels, respectively, as the broad excitation peak of FITC at 490 nm overlaps well with the $^5D_4 \rightarrow {}^7F_6$ emission of Tb^{3+} at 491 nm (see Figure S17). By the use of biotinylated NPs and FITC-labeled avidin, TR-FRET was built in the avidin–biotin system. Thus, the excitation energy was transferred from CaF_2 NPs to nearby FITC as a result of the specific binding between avidin and biotin. The principle behind the homogeneous TR-FRET assay is illustrated in Figure 4a. The concentration of avidin can be quantified by measuring the ratio of the integrated PL intensities of FITC and Tb^{3+}, as denoted by $FITC_{520}/Tb_{491}$: a value of merit derived from the deconvolution of the TR-FRET spectrum (see Figure S18). The gradual enhancement of the $FITC_{520}$ TR-FRET signal at the expense of the Tb_{491} signal as the amount of avidin increased (Figure 4b) verified the specific binding as well as the occurrence of FRET. In nonbinding control experiments, the biotinylated NPs (or FITC-labeled avidin) were replaced with nonbiotinylated NPs (or FITC-labeled BSA) under otherwise identical conditions. Since no specific binding occurred between AEP and avidin (or

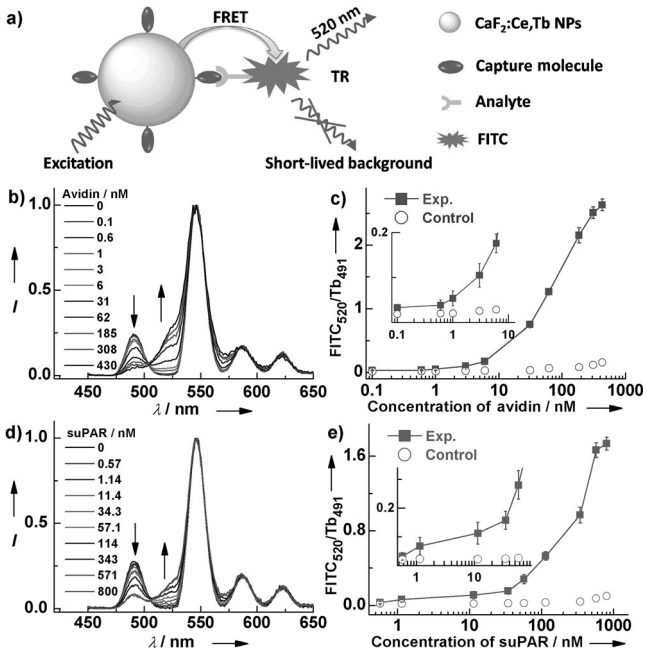

Figure 4. a) Schematic illustration showing the principle behind TR-FRET detection. b) TR-FRET spectra of the bioassay with biotinylated CaF_2:Ce,Tb NPs as bioprobes as a function of the avidin concentration. c) Calibration curve for TR-FRET detection: $FITC_{520}/Tb_{491}$ ratio of the integrated PL intensities versus the concentration of avidin. The control experiments were conducted with nonbiotinylated NPs as bioprobes. d) TR-FRET spectra of the bioassay with ATF-coupled CaF_2:Ce,Tb NPs as bioprobes as a function of the suPAR concentration. e) Calibration curve for TR-FRET detection: $FITC_{520}/Tb_{491}$ versus the concentration of suPAR. The control experiments were conducted with non-ATF-coupled NPs as bioprobes. All spectra in (b) and (d) were normalized at the maximum emission peak at 546 nm.

between biotin and BSA), the NPs and FITC were far apart in the solution, and thus no FRET occurred. The negligibly low $FITC_{520}$ TR-FRET signal detected (see Figure S19) indicated the high specificity of the TR-FRET assay. The calibration curve plotted for avidin concentrations between 0.1 and 430 nM shows that the TR-FRET signal of $FITC_{520}/Tb_{491}$ gradually increases with the avidin concentration but tends to saturate at concentrations above 308 nM (Figure 4c). The LOD derived from the calibration curve was approximately 164 pM, which is the lowest detection limit ever reported for UC- or TR-FRET bioprobes based on Ln^{3+}-doped inorganic NPs (see Table S3). The remarkable improvement in the LOD can be attributed to the long-lived luminescence (ca. 12.5 ms) and small particle size (ca. 3.8 nm) of CaF_2:Ce,Tb NPs that are advantageous in distance-dependent TR-FRET biodetection.

Owing to the high detection sensitivity and separation-free convenience of the homogeneous TR-FRET assay, we further employed this system for the detection of soluble uPAR (suPAR) with ATF-coupled NPs as TR-FRET probes. The concentration of suPAR is quantified by the TR-FRET signal of $FITC_{520}/Tb_{491}$. The $FITC_{520}$ was gradually enhanced along with a decrease in the Tb_{491} signal as the amount of suPAR was inceased (Figure 4d). This trend verifies the specific binding between ATF and suPAR and the occurrence of FRET. By contrast, in control experiments in which non-ATF-coupled NPs (or FITC-labeled BSA) were used in place of ATF-coupled NPs (or FITC-labeled suPAR) under otherwise identical conditions, the TR-FRET signal was hardly observed; this result indicates the specific binding between suPAR and ATF (see Figure S20). The calibration curve plotted for suPAR concentrations in the range of 0.5–800 nM shows that the TR-FRET signal of $FITC_{520}/Tb_{491}$ increases gradually with the suPAR concentration and saturates when the concentration exceeds 571 nM (Figure 4e). The LOD was determined to be approximately 328 pM, which is comparable to the suPAR level in the serum of cancer patients.[10b] These results indicate that ultrasmall CaF_2:Ce,Tb NPs may serve as sensitive TR-FRET bioprobes for the detection of trace amounts of tumor markers such as suPAR.

By using ATF-coupled CaF_2:Ce,Tb NPs, we designed a proof-of-concept experiment for uPAR-targeted cellular imaging. Human lung cancer cells (H1299) with uPAR overexpressed were selected as the target cancer cells, and the specific recognition capability of ATF-coupled NPs was examined by means of confocal laser scanning microscopy (CLSM). Owing to the high binding affinity between ATF and uPAR, ATF-coupled NPs can be specifically targeted to H1299 cells after coincubation in a culture medium at 37 °C for 2 h. As a result, bright green PL (green channel) of Tb^{3+} was observed on the H1299 cells upon excitation with a laser at 488 nm (Figure 5a). We also recorded bright-field images and blue-channel images, which showed the location of the 4′,6-diamidino-2-phenylindole-stained (DAPI-stained) cell nuclei of the H1299 cells. An overlay of the green-channel, blue-channel, and bright-field images showed unambiguously that the bright Tb^{3+} signal originated from ATF-coupled NPs bound to H1299 cells (Figure 5a). For comparison, a control CLSM imaging experiment was carried out on human embryo lung fibroblast (HELF) cells, in which the expression of uPAR is low, under identical imaging conditions. The green PL of Tb^{3+} was hardly observed on HELF cells due to the lack of specific recognition between ATF-coupled NPs and HELF cells (Figure 5b; see also Figure S21). When we used ATF-

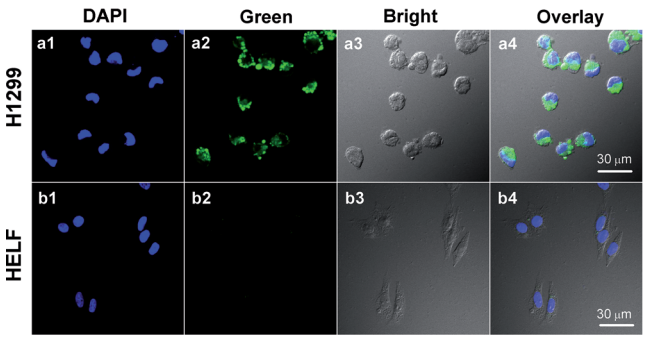

Figure 5. CLSM images of a) H1299 and b) HELF cells after incubation with ATF-coupled CaF_2:Ce,Tb NPs (0.5 mg mL^{-1}) at 37 °C for 2 h. The DAPI blue images (λ_{em} = 450–490 nm, λ_{ex} = 405 nm) indicate the nuclear regions. Intense green PL of Tb^{3+} (λ_{em} = 500–560 nm, λ_{ex} = 488 nm) was observed almost exclusively in the H1299 cells. The bright-field images outline the position of the cells. For each of the cell types, the green-channel, blue-channel, and bright-field images are overlayed for direct comparison on the far right.

coupled CaF_2:Yb,Tm@CaF_2 core/shell NPs for targeted UCL imaging, we also observed intense UCL of Tm^{3+} on H1299 cells (see Figure S22). The dark cytotoxicity, phototoxicity, and real-time cytotoxicity of ATF-coupled NPs were further assessed on HELF cells by means of cell-counting-kit (CCK-8) and electric cell–substrate impedance sensing (ECIS) assays.[14] The cell viability was determined to be larger than 90% even at a NP concentration as high as 500 $\mu g\,mL^{-1}$ (see Figure S23). This high cell viability infers that ultrasmall CaF_2:Ln^{3+} nanoprobes are biocompatible and nearly nontoxic to live cells. Our results demonstrate that CaF_2:Ln^{3+} NPs modified with specific capture molecules like ATF for tumor-marker can be used as bioprobes in the targeted imaging of cancer cells on the basis of DS or UC luminescence.

In summary, we have fabricated monodisperse and highly emissive sub-10 nm CaF_2:Ln^{3+} core-only and core/shell NPs through sodium codoping. The long-lived luminescence of Ln^{3+} and the small size of the NPs led to record-low LODs of 164 and 48 pM for the detection of avidin in homogeneous TR-FRET and heterogeneous TRPL bioassays, respectively. Furthermore, we employed ATF-coupled CaF_2:Ce,Tb NPs as sensitive TR-FRET probes for the detection of the important tumor marker suPAR with a low LOD of 328 pM, which is comparable to the suPAR level in the serum of cancer patients. We also demonstrated the successful use of CaF_2:Ln^{3+} NPs in the uPAR-targeted DS- and UC-luminescence imaging of cancer cells. These findings reveal the great potential of ultrasmall CaF_2:Ln^{3+} nanoprobes in practical bioassays for cancer diagnosis. The synthetic approach we propose can be further extended to the synthesis of other ultrasmall Ln^{3+}-doped alkaline-earth fluoride nanoprobes, such as SrF_2 and BaF_2 (see Figures S24 and S25).

Received: March 25, 2013
Published online: May 9, 2013

Keywords: calcium fluoride · lanthanides · nanoprobes · photoluminescence · tumor markers

[1] a) H. H. Gorris, O. S. Wolfbeis, *Angew. Chem.* **2013**, *125*, 3668 – 3686; *Angew. Chem. Int. Ed.* **2013**, *52*, 3584 – 3600; b) L. L. Li, P. Wu, K. Hwang, Y. Lu, *J. Am. Chem. Soc.* **2013**, *135*, 2411 – 2414; c) Y. L. Dai, P. A. Ma, Z. Y. Cheng, X. J. Kang, X. Zhang, Z. Y. Hou, C. X. Li, D. M. Yang, X. F. Zhai, J. Lin, *ACS Nano* **2012**, *6*, 3327 – 3338; d) Q. Liu, T. S. Yang, W. Feng, F. Y. Li, *J. Am. Chem. Soc.* **2012**, *134*, 5390 – 5397; e) B. Yan, J. C. Boyer, D. Habault, N. R. Branda, Y. Zhao, *J. Am. Chem. Soc.* **2012**, *134*, 16558 – 16561; f) M. E. Lim, Y. L. Lee, Y. Zhang, J. J. H. Chu, *Biomaterials* **2012**, *33*, 1912 – 1920; g) M. Haase, H. Schäfer, *Angew. Chem.* **2011**, *123*, 5928 – 5950; *Angew. Chem. Int. Ed.* **2011**, *50*, 5808 – 5829; h) D. E. Achatz, R. J. Meier, L. H. Fischer, O. S. Wolfbeis, *Angew. Chem.* **2011**, *123*, 274 – 277; *Angew. Chem. Int. Ed.* **2011**, *50*, 260 – 263; i) L. Cheng, K. Yang, Y. G. Li, J. H. Chen, C. Wang, M. W. Shao, S. T. Lee, Z. Liu, *Angew. Chem.* **2011**, *123*, 7523 – 7528; *Angew. Chem. Int. Ed.* **2011**, *50*, 7385 – 7390; j) H. Zhang, Y. Li, I. A. Ivanov, Y. Qu, Y. Huang, X. Duan, *Angew. Chem.* **2010**, *122*, 2927 – 2930; *Angew. Chem. Int. Ed.* **2010**, *49*, 2865 – 2868; k) J. W. Wang, P. A. Tanner, *J. Am. Chem. Soc.* **2010**, *132*, 947 – 949; l) K. Ai, B. Zhang, L. Lu, *Angew. Chem.* **2009**, *121*, 310 – 314; *Angew. Chem. Int. Ed.* **2009**, *48*, 304 – 308; m) Y. S. Liu, D. T. Tu, H. M. Zhu, X. Y. Chen, *Chem. Soc. Rev.* **2013**, DOI: 10.1039/C3CS60060B.

[2] a) A. D. Ostrowski, E. M. Chan, D. J. Gargas, E. M. Katz, G. Han, P. J. Schuck, D. J. Milliron, B. E. Cohen, *ACS Nano* **2012**, *6*, 2686 – 2692; b) X. D. Wang, J. A. Stolwijk, T. Lang, M. Sperber, R. J. Meier, J. Wegener, O. S. Wolfbeis, *J. Am. Chem. Soc.* **2012**, *134*, 17011 – 17014; c) M. Longmire, P. L. Choyke, H. Kobayashi, *Nanomedicine* **2008**, *3*, 703 – 717.

[3] Y. S. Liu, D. T. Tu, H. M. Zhu, E. Ma, X. Y. Chen, *Nanoscale* **2013**, *5*, 1369 – 1384.

[4] a) X. Teng, Y. H. Zhu, W. Wei, S. C. Wang, J. F. Huang, R. Naccache, W. B. Hu, A. I. Y. Tok, Y. Han, Q. C. Zhang, Q. L. Fan, W. Huang, J. A. Capobianco, L. Huang, *J. Am. Chem. Soc.* **2012**, *134*, 8340 – 8343; b) Q. Q. Su, S. Y. Han, X. J. Xie, H. M. Zhu, H. Y. Chen, C. K. Chen, R. S. Liu, X. Y. Chen, F. Wang, X. G. Liu, *J. Am. Chem. Soc.* **2012**, *134*, 20849 – 20857; c) N. J. J. Johnson, A. Korinek, C. H. Dong, F. C. J. M. van Veggel, *J. Am. Chem. Soc.* **2012**, *134*, 11068 – 11071; d) F. Zhang, R. C. Che, X. M. Li, C. Yao, J. P. Yang, D. K. Shen, P. Hu, W. Li, D. Y. Zhao, *Nano Lett.* **2012**, *12*, 2852 – 2858; e) Q. Liu, Y. Sun, T. S. Yang, W. Feng, C. G. Li, F. Y. Li, *J. Am. Chem. Soc.* **2011**, *133*, 17122 – 17125; f) G. A. Ozin, N. Bogdan, F. Vetrone, J. A. Capobianco, *Nano Lett.* **2011**, *11*, 835 – 840; g) H. X. Mai, Y. W. Zhang, R. Si, Z. G. Yan, L. D. Sun, L. P. You, C. H. Yan, *J. Am. Chem. Soc.* **2006**, *128*, 6426 – 6436; h) S. Heer, K. Kompe, H. U. Gudel, M. Haase, *Adv. Mater.* **2004**, *16*, 2102 – 2105.

[5] a) Y. L. Dai, C. M. Zhang, Z. Y. Cheng, P. A. Ma, C. X. Li, X. J. Kang, D. M. Yang, J. Lin, *Biomaterials* **2012**, *33*, 2583 – 2592; b) G. Y. Chen, J. Shen, T. Y. Ohulchanskyy, N. J. Patel, A. Kutikov, Z. P. Li, J. Song, R. K. Pandey, H. Agren, P. N. Prasad, G. Han, *ACS Nano* **2012**, *6*, 8280 – 8287; c) Y. F. Wang, L. D. Sun, J. W. Xiao, W. Feng, J. C. Zhou, J. Shen, C. H. Yan, *Chem. Eur. J.* **2012**, *18*, 5558 – 5564; d) N.-N. Dong, M. Pedroni, F. Piccinelli, G. Conti, A. Sbarbati, J. E. Ramírez-Hernández, L. Martínez-Maestro, M. C. Iglesias-de la Cruz, F. Sanz-Rodriguez, A. Juarranz, F. Chen, F. Vetrone, J. A. Capobianco, J. García Sole, M. Bettinelli, D. Jaque, A. Speghini, *ACS Nano* **2011**, *5*, 8665 – 8671; e) G. F. Wang, Q. Peng, Y. D. Li, *J. Am. Chem. Soc.* **2009**, *131*, 14200 – 14201.

[6] F. Wang, J. A. Wang, X. G. Liu, *Angew. Chem.* **2010**, *122*, 7618 – 7622; *Angew. Chem. Int. Ed.* **2010**, *49*, 7456 – 7460.

[7] D. Q. Chen, Y. L. Yu, F. Huang, P. Huang, A. P. Yang, Y. S. Wang, *J. Am. Chem. Soc.* **2010**, *132*, 9976 – 9978.

[8] a) J. C. G. Bunzli, S. V. Eliseeva, *Chem. Sci.* **2013**, *4*, 1939 – 1949; b) Q. Ju, Y. S. Liu, D. T. Tu, H. M. Zhu, R. F. Li, X. Y. Chen, *Chem. Eur. J.* **2011**, *17*, 8549 – 8554; c) J. F. Lemonnier, L. Guénée, C. Beuchat, T. A. Wesolowski, P. Mukherjee, D. H. Waldeck, K. A. Gogick, S. Petoud, C. Piguet, *J. Am. Chem. Soc.* **2011**, *133*, 16219 – 16234; d) J. C. G. Bünzli, *Chem. Rev.* **2010**, *110*, 2729 – 2755.

[9] a) Y. S. Liu, S. Y. Zhou, D. T. Tu, Z. Chen, M. D. Huang, H. M. Zhu, E. Ma, X. Y. Chen, *J. Am. Chem. Soc.* **2012**, *134*, 15083 – 15090; b) Q. Ju, D. T. Tu, Y. S. Liu, R. F. Li, H. M. Zhu, J. C. Chen, Z. Chen, M. D. Huang, X. Y. Chen, *J. Am. Chem. Soc.* **2012**, *134*, 1323 – 1330; c) D. T. Tu, L. Q. Liu, Q. Ju, Y. S. Liu, H. M. Zhu, R. F. Li, X. Y. Chen, *Angew. Chem.* **2011**, *123*, 6430 – 6434; *Angew. Chem. Int. Ed.* **2011**, *50*, 6306 – 6310.

[10] a) F. Blasi, P. Carmeliet, *Nat. Rev. Mol. Cell Biol.* **2002**, *3*, 932 – 943; b) Q. Huai, A. P. Mazar, A. Kuo, G. C. Parry, D. E. Shaw, J. Callahan, Y. D. Li, C. Yuan, C. B. Bian, L. Q. Chen, B. Furie, B. C. Furie, D. B. Cines, M. D. Huang, *Science* **2006**, *311*, 656 – 659.

[11] L. B. Su, J. Xu, H. J. Li, W. Q. Yang, Z. Q. Zhao, J. L. Si, Y. J. Dong, G. Q. Zhou, *Opt. Lett.* **2005**, *30*, 1003 – 1005.

[12] A. G. Dong, X. C. Ye, J. Chen, Y. J. Kang, T. Gordon, J. M. Kikkawa, C. B. Murray, *J. Am. Chem. Soc.* **2011**, *133*, 998 – 1006.

[13] a) X. Zeng, Y. X. Sun, W. Qu, X. Z. Zhang, R. X. Zhuo, *Biomaterials* **2010**, *31*, 4771 – 4780; b) R. J. Goodson, M. V. Doyle, S. E. Kaufman, S. Rosenberg, *Proc. Natl. Acad. Sci. USA* **1994**, *91*, 7129 – 7133.
[14] a) L. M. Wang, Y. Liu, W. Li, X. M. Jiang, Y. L. Ji, X. C. Wu, L. G. Xu, Y. Qiu, K. Zhao, T. T. Wei, Y. F. Li, Y. L. Zhao, C. Y. Chen, *Nano Lett.* **2011**, *11*, 772 – 780; b) L. S. Li, Z. P. Luo, Z. Chen, J. C. Chen, S. Y. Zhou, P. Xu, P. Hu, J. D. Wang, N. S. Chen, J. L. Huang, M. D. Huang, *Bioconjugate Chem.* **2012**, *23*, 2168 – 2172.

